RESEARCH ARTICLE

From widespread faulting to localised rifting: Evidence from K-Ar fault gouge dates from the Norwegian North Sea rift shoulder

Haakon Fossen[1,2] 🟢 | Anna K. Ksienzyk[2,3] | Atle Rotevatn[2] 🟢 | Marit S. Bauck[4] | Klaus Wemmer[5]

[1]Natural History Collections, University of Bergen, Bergen, Norway

[2]Department of Earth Science, University of Bergen, Bergen, Norway

[3]Geological Survey of Norway, Trondheim, Norway

[4]Department of Geosciences, University of Oslo, Oslo, Norway

[5]Geoscience Center, Georg-August University, Göttingen, Germany

Correspondence

Haakon Fossen, Natural History Collections, University of Bergen, Box 7800, 5020 Bergen Norway.
Email: haakon.fossen@uib.no

Abstract

Although seismic and stratigraphic well information put tight constraints on rift basin evolution, eroded rift shoulders commonly expose polydeformed prerift basement whose deformation history may be difficult to constrain. In this work, we apply K-Ar dating of fault gouge samples from 18 faults to explore the brittle deformation of the well-exposed eastern rift margin to the northern North Sea rift. We find evidence of clay gouge formation since the Late Devonian, with distinct Permian and Jurassic fault activity peaks that closely match early stages of the two well-established North Sea rift phases. A marked decay in fault density away from the rift margin confirms a close relationship between rifting and onshore faulting. The results show that initial rift-related extension affected a much wider area than the resulting offshore rift. Hence our data support a rift model where strain is initially distributed over a several 100 km wide region, as a prelude to the development of the ~150–200 km wide Permo-Triassic northern North Sea rift as defined by large marginal faults. Towards the end of the second rift phase, strain localises even more strongly to the 25–50 km wide Viking Graben. Interestingly, a period of early widespread extension is seen for both phases of North Sea rifting and may be a general characteristic of continental rifting. The documented prerift faulting and fracturing of the basement since the Devonian weakened the basement and probably facilitated the widespread initial extension that subsequently localised to form the northern North Sea rift, with further localisation to its relatively narrow central part (Viking Graben).

KEYWORDS

fault gouge dating, incipient rifting, North Sea rift, rift margin deformation

1 | INTRODUCTION

Continental rifts are built on a continental crust that during rifting undergoes a history of stretching, thinning and subsidence. The overall rift history is well recorded by the basin fill and its stratigraphic relations to faults and fault activity, but how and to what extent this deformation was accommodated by the basement and the role of prerift structures may be less clear. Exhumed rift margins commonly expose the basement with its prerift structure but may be difficult

or time-consuming to assess in terms of rift-related faulting and structural reactivation. In this work, we explore brittle faulting in the crystalline Caledonian and Proterozoic crust of SW Norway, immediately east of the northern North Sea rift. This area (Figure 1) is crisscrossed by faults and fractures that, apart from postdating Caledonian (Ordovician-Early Devonian) ductile deformation structures, are poorly constrained in terms of age (e.g. Braathen, 1999; Fossen et al., 2016; Gabrielsen et al., 2002; Ksienzyk et al., 2016; Larsen et al., 2003). Unresolved questions include: To what extent was the basement affected by faulting prior to rift initiation in the Permian? How much of the onshore faulting is related to the North Sea rifting, and how far away from the rift can we trace the signature of rifting? And what can our knowledge of onshore basement tell us about the poorly known crystalline basement underneath the northern North Sea Rift fill? To address these questions, we present K-Ar dates of 18 fault gouge samples from the Sognefjord-Nordfjord area and combine those results with published data from the Bergen and Bømlo areas to the south (Figure 1). Based on the total dataset we demonstrate that rift-related extension affected the basement far into the onshore rift margin and that this wide-spread extension and related faulting predated the main rift event.

2 | GEOLOGIC SETTING

Southwest Norway represents the east margin of the northern North Sea rift (Figure 2). It exposes Proterozoic Baltican crust and overlying lower Paleozoic metasedimentary rocks that were reworked during the Caledonian orogeny and allochthonous Caledonian units of continental margin and oceanic affinity. Also preserved are post-Caledonian Devonian basins in the hanging wall of the Nordfjord-Sogn Detachment Zone (NSDZ) – the largest of several Devonian extensional shear zones that formed immediately after the Caledonian collisional history (Fossen, 2010).

The northern North Sea rift basin formed during a two-phase rift history that is well known from about 50 years of extensive hydrocarbon exploration. The first rift basins initiated in the Permian with an Early Triassic climax, followed by a Middle to Late Jurassic phase that locally extended into the Early Cretaceous (Færseth, 1996; Roberts et al., 1995; Steel & Ryseth, 1990). A thick postrift sequence was deposited between the two rift phases. Some faults show evidence of tectonic activity also during this period, implying that rifting was not completely turned off during this Middle Triassic to Middle Jurassic period (Deng et al., 2017; Ravnås et al., 2000). In the Early Cretaceous, rifting was focused along the future North Atlantic margin north and west of the northern North Sea rift, with important rift stages in the Early Cretaceous, middle Cretaceous and Paleocene, culminating

Highlights

- North Sea rifting followed an initial low-strain phase of widely distributed extension
- K-Ar dating of fault gouge reveals extension >100 km into the rift shoulder
- Reactivation of basement structures was widespread during early stages of rifting

in the continental breakup in the early Eocene (e.g. Doré et al., 1999).

East of the Viking Graben, in the offshore Horda Platform area near the coast (Figure 1), most of the faulting occurred during the Permo-Triassic (first) rift phase, with normal offsets up to several kilometres (Figure 1, profile). In contrast, the second rift phase involved much less strain and smaller displacements on reactivated faults (Bell et al., 2014; Færseth, 1996; Odinsen et al., 2000; Phillips et al., 2019). North of 61°N, in the Måløy Slope area, the situation is different: Here the rifting appears to be almost entirely Jurassic-Early Cretaceous, with the Permo-Triassic extension and deposits occurring farther west. The absence of Permo-Triassic rifting in this area can be documented from seismic and supporting well data (Figure 3). These data show Jurassic sediments deposited directly on the crystalline basement, with the total basement fault offsets accommodating Jurassic-Cretaceous synrift deposits. The expansion of the sedimentary cover in the hanging wall to the main fault in Figure 3 shows that faulting occurred from the Middle Jurassic and far into the Cretaceous.

Onshore southwestern Norway, the prerift basement is dissected by numerous post-Caledonian extensional faults showing a wide range in orientation (Braathen, 1999; Fossen, 1998; Fossen et al., 2016; Gabrielsen et al., 2002; Ksienzyk et al., 2016; Larsen et al., 2003). Coast-parallel faults are particularly well represented, together with NE and NW trends (Fossen et al., 2016). Some of the largest faults formed partly or fully by the reactivation of Devonian extensional shear zones at brittle crustal depths, notably the low-angle Lærdal-Gjende and Dalsfjord faults that are discussed below. However, the majority of the brittle faults are steeper and crosscut all ductile structures. The general absence of post-Middle Devonian stratigraphic markers makes it difficult to constrain the age of these structures beyond the fact that they postdate Early Devonian ductile fabrics.

An interpretation of lineaments, from digital elevation models and bathymetric data (~10 m resolution) and Google Earth imagery, is shown in Figure 4. This lineament map was produced by the manual tracing of lineaments longer than roughly 1 km and is biased by the manual lineament
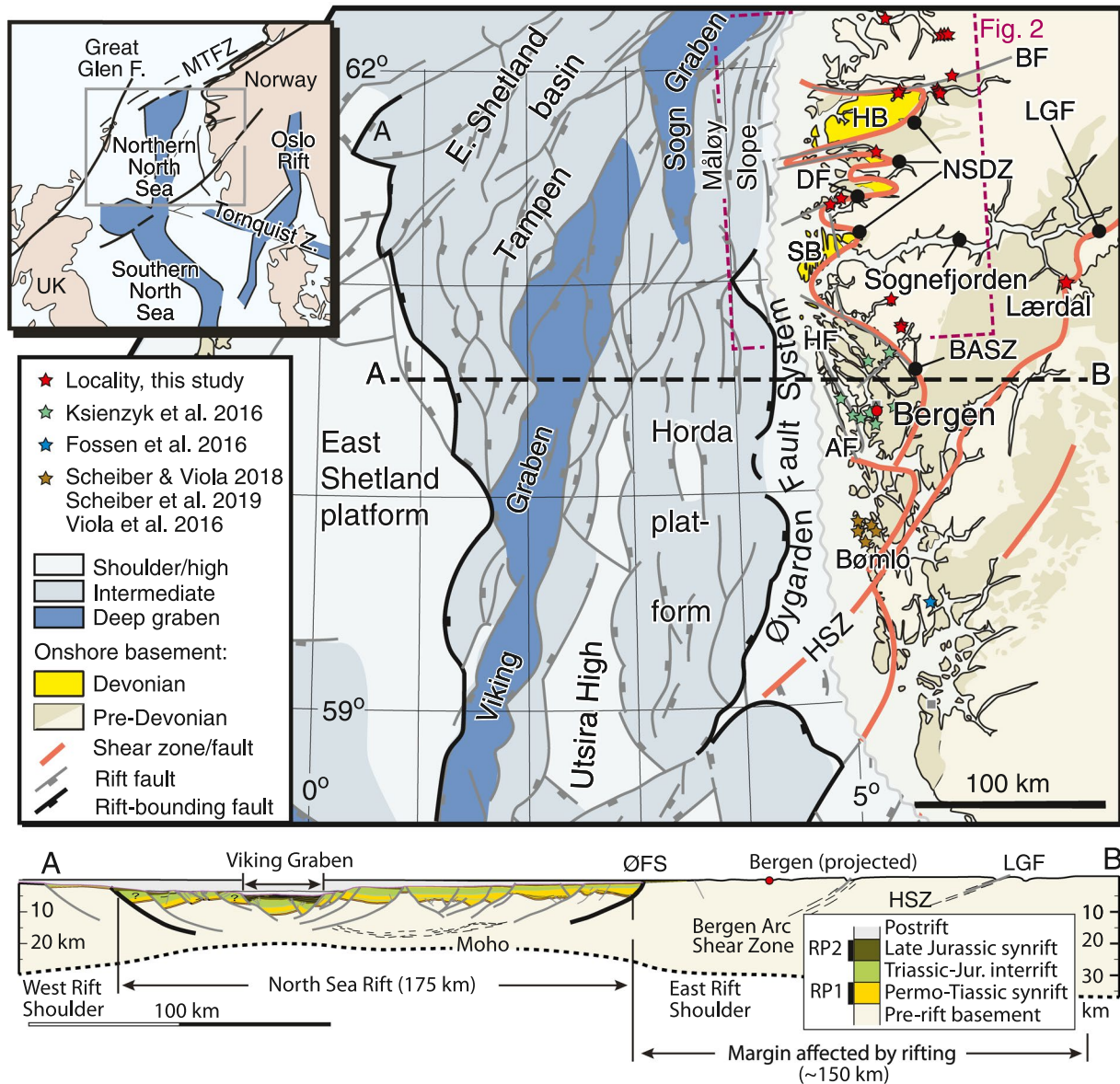
FIGURE 1 Structural setting of the northern North Sea rift and its eastern shoulder. Cross-section based on offshore 3D seismic data, except for the westernmost part which is uncertain. Sampling localities are indicated. Red lines are Devonian shear/fault zones reactivated at later stages. AF, Austefjord Fault; BASZ, Bergen Arc Shear Zone; BF, Bortnen Fault; DF, Dalsfjord Fault; HSZ, Hardangerfjord Shear Zone; HF, Hjeltefjord Fault; HB, Hornelen Basin; LGF, Lærdal-Gjende Fault; NSDZ, Nordfjord-Sogn Detachment System; RP, Rift Phase; SB, Solund Basin; ØFS, Øygarden Fault System

identification and variations in lithology and exposure, although the degree of exposure at this scale is good in all parts of the region, particularly at high elevations. Our five profiles in Figure 4 show an increase in fault density towards the coast, with a coastal density that is 5–8 times higher than 100 km into the mainland. This is consistently expressed by each profile, suggesting that this increase towards the rift is real, at least qualitatively. The observation, therefore, suggests that the majority of the faults along the coast are rift related. Most of these lineaments represent faults with slip surfaces, many with only metres to tens of metres of displacement, but some with larger displacements. Where well exposed, these faults

typically show a zone of cataclasite and an internal zone of incohesive fault gouge. Cohesive fault rocks (cataclasites) are generally assumed to represent deep upper crustal formation, and incohesive fault gouge represents shallower (0–4 km) deformation (Sibson, 1977). Regionally, however, K-Ar fault gouge illite ages as old as late Devonian/early Carboniferous (this work) and cohesive cataclastic fault rocks as young as Jurassic/Cretaceous (^{40}Ar/^{39}Ar dating: Eide et al., 1997; paleomagnetic dating: Andersen et al., 1999) occur. Therefore, this assumption may work with respect to relative ages at the outcrop scale, but it cannot be used as an absolute criterion for depth or age of faulting.
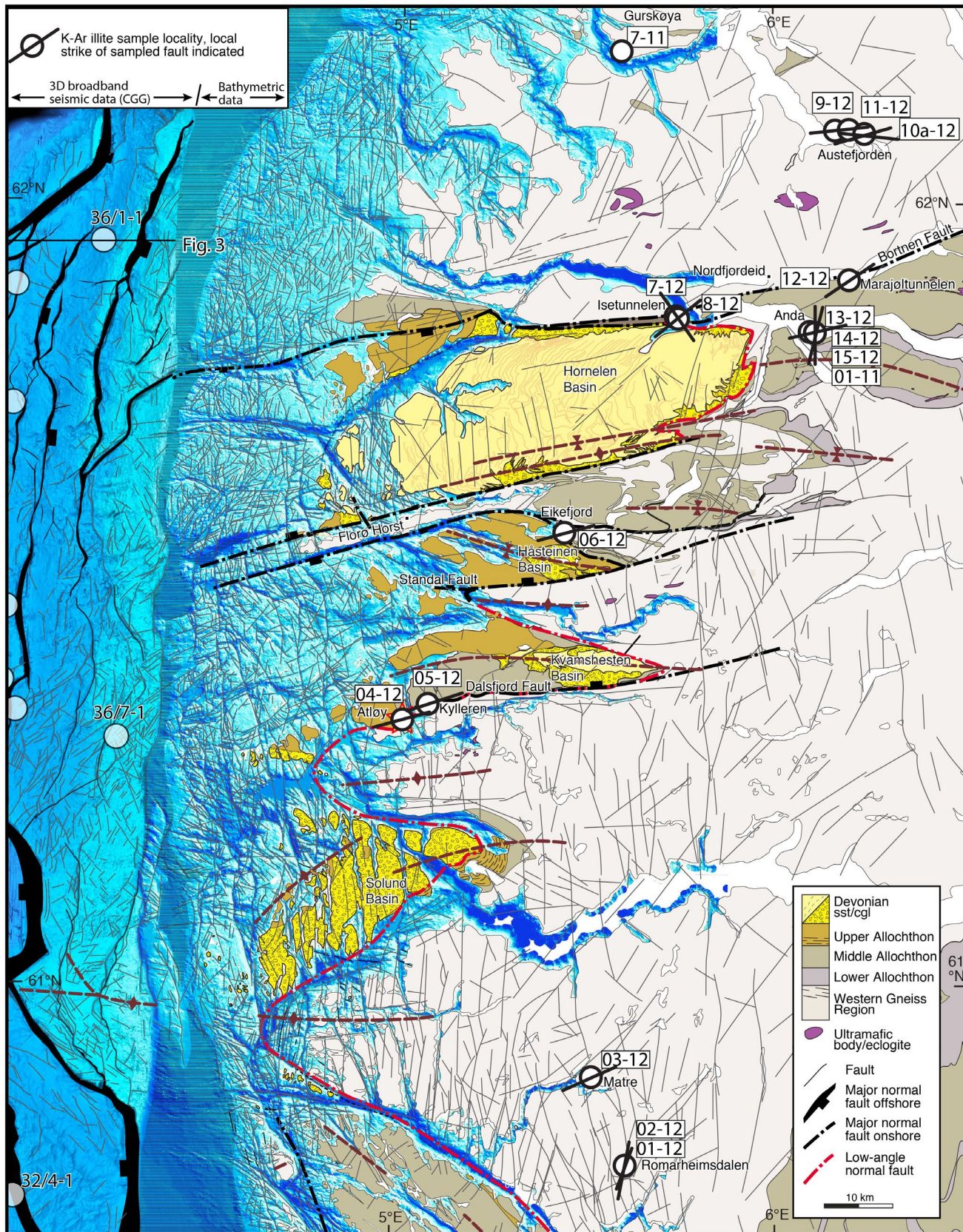
FIGURE 2 Map of the onshore geology and near-shore top crystalline basement fault pattern connected by bathymetric data along the coast (see Figure 1 for location). Fault gouge sample locations are shown with local fault orientations indicated. Fault interpretation is based on an onshore 10 m elevation model and field observations, bathymetry data (Olex), and marine seismic 3D data (CGG) in the western part. Note that the Nordfjord Sogn Detachment Zone is a several km-thick shear zone below (east of) the Devonian basins, whereas the red dashed line merely represents brittle faulting in the upper part of this zone. Note that only prominent onshore faults/lineaments are shown here. See Figure 4 for a comprehensive interpretation of onshore structures
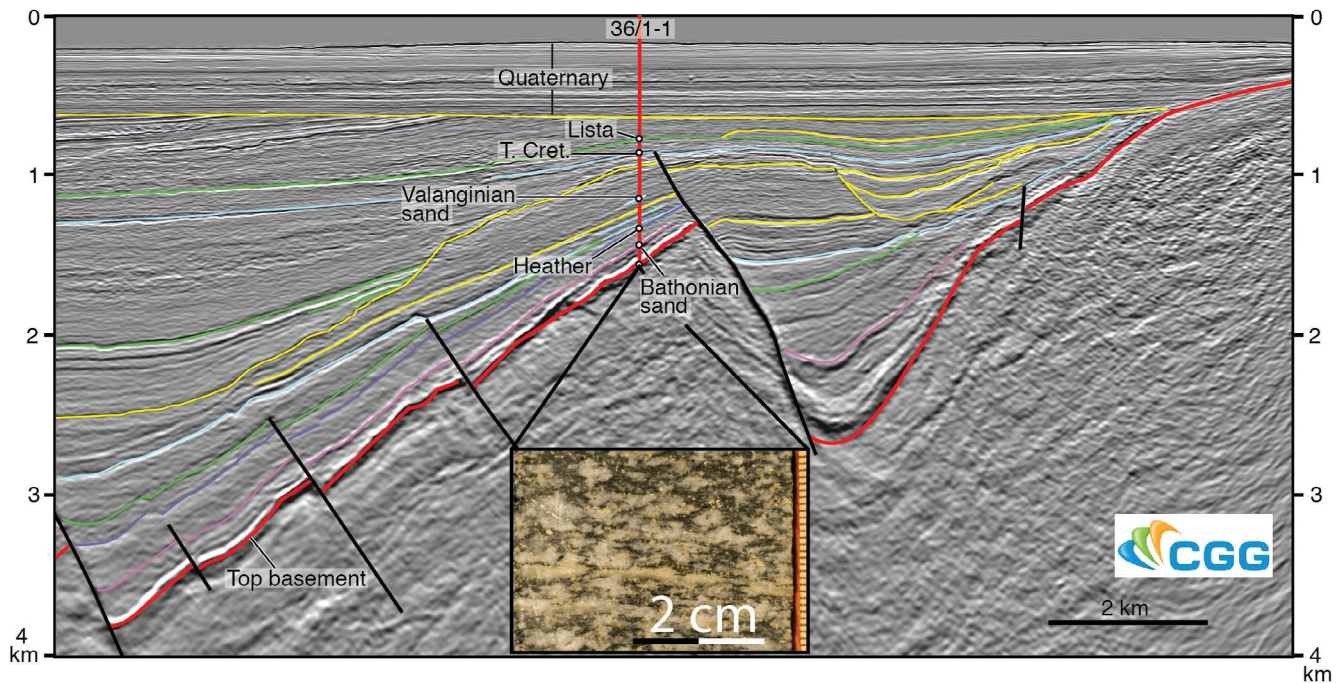
FIGURE 3 Seismic line through well 36/1-1 in the Måløy Slope (see Figure 2 for location), showing Middle Jurassic overlaying crystalline basement (red colour). Photo of the cored crystalline basement is shown. The small faults show similar offsets at top basement and Jurassic levels. The main fault east of well 36/6-1 holds a hanging-wall growth sequence that constrains the entire fault history from Middle Jurassic to Cretaceous. No evidence of pre-Jurassic faulting is seen

3 | K-AR DATING METHODOLOGY AND INTERPRETATION APPROACH

K-Ar and ^{40}Ar/^{39}Ar analyses of fault gouge samples have become well-established dating methods for clay-gouge bearing brittle faults (e.g. Bense et al., 2014; Ksienzyk et al., 2016; Löbens et al., 2011; Torgersen et al., 2014; van der Pluijm et al., 2001; Viola et al., 2016; Vrolijk et al., 2018; Zwingmann & Mancktelow, 2004; Zwingmann et al., 2010). We applied the K-Ar method to 18 faults sampled in relatively fresh quarries, road cuts or tunnel sections along the coast of SW Norway and up to 150 km inland (see Figure 2 and Supplementary information for sample locations). Three grain-size fractions (2–6, <2 and <0.2 μm) were analysed for each sample, according to analytical procedures presented in the Supporting information.

When several grain size fractions separated from a fault gouge sample are dated, they often display a range of ages, where the ages typically correlate with grain size, i.e. the coarsest dated gain size fraction gives the oldest age (e.g. Ksienzyk et al., 2016; Löbens et al., 2011; Solum et al., 2005; Torgersen et al., 2014; van der Pluijm, 2001; Zwingmann, Mancktelow, et al., 2010). Several processes may contribute to produce such inclined age spectra. Thermally activated volume diffusion of radiogenic ^{40}Ar can reset K-Ar ages in fault gouges (e.g. Uysal et al., 2006; Zwingmann et al., 2010), but is unlikely to affect even the finest grain size fraction at a temperature below 250°C (e.g. Torgersen

et al., 2014). Hence, the two main processes that need to be considered are mixing with older K-bearing minerals (e.g. muscovite, K-feldspar, hornblende) inherited from the host rock (Torgersen et al., 2014, 2015; Zwingmann, Mancktelow, et al., 2010) or fault reactivation producing two or more generations of authigenic illite (Bense et al., 2014; Torgersen et al., 2014; Viola et al., 2016).

At the root of the problem lies the impracticality of physically separating authigenic illite, the target mineral for K-Ar dating, from other fine-grained components of the fault gouge. Physically separating different generations of illite that might have grown in a fault is even less achievable. As a consequence, almost all separated grain size fractions are a mixture of minerals that can either be inherited from the host rock or neocrystallised in the fault. All minerals that contain potassium will contribute to the K-Ar date, and thus many fault gouge fine-fraction ages are, to a greater or lesser degree, mixed ages that require careful evaluation to decrypt the age of one or more periods of fault activity versus the influence of inherited host rock minerals (e.g. Torgersen et al., 2015; Viola et al., 2016; Vrolijk et al., 2018).

The presence of inherited K-bearing minerals can be determined by routine XRD analyses. K-feldspar and hornblende are easily identified, whereas muscovite, due to its similarity to illite, is more challenging to detect but may be distinguished from authigenic illite by its higher crystallinity (lower Kübler Index) or different polytypes (e.g. Löbens et al., 2011; van der Pluijm et al., 2001; Vrolijk et al., 2018).
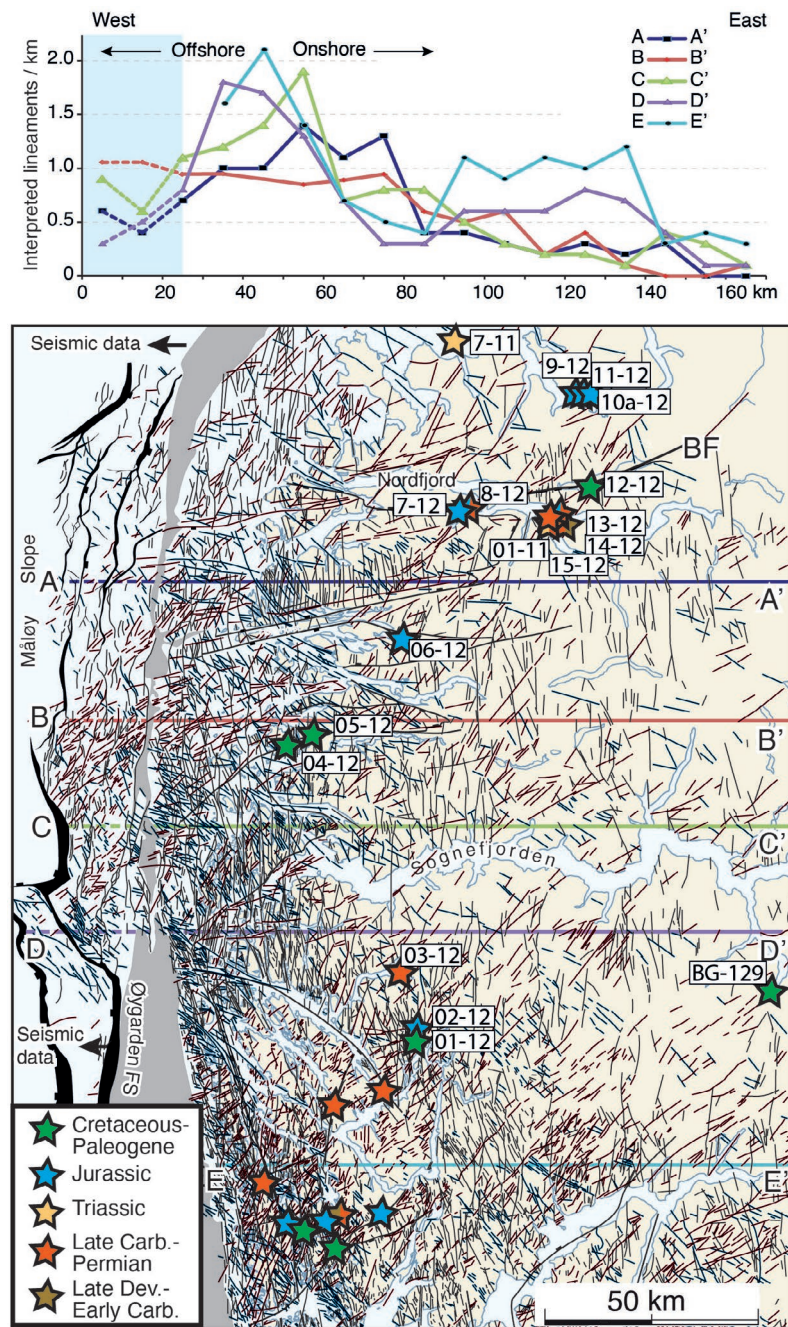
FIGURE 4 Onshore lineament map, based on Google Earth imagery and assisted by a 10 m elevation model onshore (gently illuminated from the W), combined with lineament interpretation from bathymetry map near-shore and broadband 3D seismic data provided by CGG offshore. Underlap between the latter two datasets is marked gray. Most lineaments represent relatively minor faults. The 5 profiles show a general increase in lineament density from the inland towards the coast. Lower density in the west is due to lower offshore data resolution. Stars indicate sample locations and are colour-coded for interpreted age of fault activity. Unnamed localities are from Ksienzyk et al. (2016). BF, Bortnen Fault

The contribution of any mineral to the age of the dated fine fraction depends on the amount of the mineral present, its K-content and age. The following generic examples demonstrate the effect of each of these three variables. They have been calculated using a mixture modelling spreadsheet (developed by R. van der Lelij, Geological Survey of Norway), that takes into account the amount, K-content and age of each mineral to estimate the effect of different mineral phases on the age of fault gouge samples:

Example (1) Mixing 95% Early Jurassic illite (200 Ma, 6 wt% K) with 5% Early Devonian K-feldspar (400 Ma, 14 wt% K), will change the age of the dated fine fraction by 12% (to 223 Ma).

Example (2) Mixing 95% Early Jurassic I/S (mixed-layer illite/smectite; 200 Ma, 1 wt% K) with 5% Early Devonian K-feldspar (400 Ma, 14 wt% K) will changes the age of the dated fine fraction by 44% (to 288 Ma). Due to the lower potassium content (cf. example 1), I/S is more vulnerable to contamination.

Example (3) Mixing 95% Early Permian illite (300 Ma, 6 wt% K) with 5% Early Devonian K-feldspar (400 Ma, 14 wt% K), will change the age of the dated fine fraction by only 4% (to 311 Ma). The smaller age difference between illite and K-feldspar (cf. example 1) diminishes the impact of contamination on the sample age.

Example (4) Mixing 95% Early Jurassic illite (200 Ma, 6 wt% K) with 5% Early Devonian hornblende (400 Ma, ~1 wt% K is the average value for representative hornblende from W-Norway; Boundy et al., 1996; Fossen & Dunlap, 1998), will change the age of the dated fine fraction by only 1% (to 202 Ma). The low K-content (cf. example 1) makes the hornblende a weaker contaminant than K-feldspar.

The ages of potentially problematic minerals from the host rock of the dated faults have been determined by several earlier studies: $^{40}Ar/^{39}Ar$ hornblende ages from West Norway range from ~420 to 395 Ma (Boundy et al., 1996; Chauvet & Dallmeyer, 1992; Fossen & Dunlap, 1998), whereas the majority of K-Ar and $^{40}Ar/^{39}Ar$ muscovite ages fall between ~420 and 385 Ma (Berry et al., 1995; Chauvet & Dallmeyer, 1992; Fossen & Dallmeyer, 1998; Fossen & Dunlap, 1998, 2006; Walsh et al., 2007; Young et al., 2011). $^{40}Ar/^{39}Ar$ K-feldspar analyses gave complex age spectra but generally slightly younger ages (Arnaud & Eide, 2000; Dunlap & Fossen, 1998; Eide et al., 1997, 1999). We have assessed the effect of inherited hornblende, K-feldspar and muscovite, when present, for each dated grain size fraction based on these known ages. If the effect is expected to be minor (within the uncertainties of the method, e.g. examples 3 and 4), the fine fraction ages are considered for further interpretation. If the effect is clearly exceeding the uncertainties of the method (2 σ typically 5%–10%; e.g. examples 1 and 2), the respective age is considered to be a mixed age and excluded from further interpretation.

Although the influence of inherited K-bearing minerals can occasionally explain the entire range of grain size fraction ages in a sample, many samples show a considerable spread in ages even after the influence of other K-bearing minerals has been ruled out or affected ages have been excluded. We interpret this to be a sign of fault reactivation where illite has either grown repeatedly or over extended periods of time, resulting in different generations of illite (e.g. Ksienzyk et al., 2016; Torgersen et al., 2014; Viola et al., 2016). Identifying different illite generations can be challenging, but may be based on discrete illite versus I/S, different illite crystallinities or different polytypes (e.g. Solum et al., 2005; Haines & van der Pluijm, 2008; Bense et al., 2014; Vrolijk et al., 2018). Although faults can be reactivated multiple times, resulting in multiple generations of illite, generally only two endmembers can be resolved, at best, in a single sample (with several grain-size fractions analysed). A more detailed reconstruction of a fault's history requires a detailed sampling of different fault domains (e.g. Scheiber et al., 2019; Viola et al., 2016). This has not been attempted in this study, which aimed to obtain a regional overview. Nevertheless, in several samples, two different illite generations can be distinguished and their effect on the age of each grain size fraction can be assessed similarly to the effect of other K-bearing mineral phases, with the

major caveat that assumptions have to be made about the age of the different illite generations. The rules described above are applied here as well: Grain size fraction ages that can with some confidence be assigned to one illite generation or are only slightly affected by mixing with another illite generation (i.e. the effect is considered to be within the uncertainties of the method) are interpreted to date illite growth in the fault. Ages where the effect of mixing of different illite generations is expected to exceed the uncertainties of the method, moreover, are rejected as mixed ages. Based on these considerations, we have assigned each K-Ar grain size fraction date to one of the following categories (Table 1): (a) Fault activity/reactivation – the age corresponds to the growth of illite or I/S during fault activity and the effect of contamination with other age components is considered to be minor. (b) Approximate fault activity/reactivation (or max./min. age fault activity/reactivation) – the age is affected by some contamination with one or more age components, but is still considered to be geologically meaningful as it can provide a maximum or minimum age for fault activity. (c) Mixed age – different age components contribute to the age to such a degree that a geologically meaningful interpretation has not been attempted. We would like to highlight once more, that some degree of contamination by either inherited wall rock minerals or different authigenic illite phases can never be ruled out entirely and thus all ages, even those in category 1, are to some degree mixed ages. However, we use these categories as a practical means to distinguish between ages where we interpret the effect of contamination to be small enough as to be geologically irrelevant (category 1), moderate (category 2) or significant enough to make a meaningful interpretation impossible (category 3).

The finest grain size fraction is generally least affected by host rock inheritance and most likely to date the last occurrence of illite growth in the fault (e.g. Torgersen et al., 2014; Viola et al., 2016). Except for a few cases where host rock inheritance or mixing with an older generation of authigenic illite can be demonstrated, we interpret the ages of the finest analysed grain size fractions (<0.2 μm in our case, <0.1 μm in Scheiber & Viola (2018); Viola et al., 2016, and Scheiber et al., (2019)) as the last episode of fault activity that caused the growth of illite or I/S and can thus be detected by the K-Ar dating method. The coarsest grain size fractions are generally most strongly affected by host rock inheritance. However, if the absence of any inherited K-bearing minerals can be demonstrated, or their influence is considered to be minor, the coarse fraction may date an earlier period of fault activity. Thus, in some faults, two periods of fault activity can be recorded in the K-Ar fault gouge data. The intermediate grain size fraction ages are most often mixed ages. However, they can occasionally overlap with the age of either the fine or coarse fraction, when illite authigenesis was extensive enough to generate illite over a larger range of grain sizes (Viola et al., 2016). When two or more grain

TABLE 1 Mineralogy, illite crystallinity and K-Ar age data of fine fractions separated from fault gouge samples

Sample / Size fraction[a]	Mineralogy[b] I/M	I/S	Kfs	Am	Chl	Qtz	Pl	Others	% Illite in I/S	Illite crystallinity[c] KI_a	KI_g	KI zone	K_2O (wt. %)	^{40}Ar*[d] (nl/g) STP	^{40}Ar* (%)	Age (Ma)	±2σ (Ma)	Interpretation[e]
GO-01-11																		
2–6 µm	+++	—	o	o	+	o	o	—	n.a.	0.38	0.37	Low anchizone	5.19	69.52	90.81	374	9	Max. age fault activity (<374 Ma)
<2 µm	+++	—	o	o	+	o	o	—	n.a.	0.43	0.42	Deep diagenetic zone	5.81	65.45	88.78	319	9	Mixed age
<0.2 µm	+++	—	o	?	+	o	o	—	n.a.	0.46	0.47	Deep diagenetic zone	5.68	55.19	87.10	279	8	Fault reactivation (ca. 279 Ma)
GO-01-12																		
2–6 µm	o	++	o	+	+++	—	—	—	~20	0.65	0.58	Deep diagenetic zone	3.14	16.87	92.23	159	3	Mixed age
<2 µm	o	+++	?	?	+++	—	—	—	20	0.57	0.54	Deep diagenetic zone	2.96	10.18	74.93	104	2	Mixed age
<0.2 µm	?	+++	—	—	++	—	—	—	20	n.a.	n.a.	Deep diagenetic zone	2.59	6.86	56.90	80	3	Fault reactivation (ca. 80 Ma)
GO-02-12																		
2–6 µm	+	+++	o	—	+	—	—	—	<10	0.40	0.41	Low anchizone	2.91	24.52	93.40	244	5	Mixed age
<2 µm	o	+++	—	—	o	—	—	FeS (?)	<10	0.46	0.50	Deep diagenetic zone	1.95	12.98	85.46	196	4	Mixed age
<0.2 µm	o	+++	—	—	o	—	—	FeS (o)	10	0.49	0.51	Deep diagenetic zone	1.77	10.18	81.19	170	4	Fault reactivation (ca. 170 Ma)
GO-03-12																		
2–6 µm	+++	+	—	—	+	+	—	—	n.a.	0.20	0.19	Epizone	4.93	52.61	98.77	304	8	Fault activity (ca. 304 Ma)
<2 µm	+++	+++	—	—	+	o	—	—	10–20	0.24	0.24	Epizone	5.99	56.94	98.75	273	5	Mixed age
<0.2 µm	++	+++	—	—	+	—	—	—	10–20	0.33	0.34	Low anchizone	4.99	35.96	96.17	211	2	Mixed age
GO-04-12																		
2–6 µm	—	+	+	—	+++	+	—	—	10	n.a.	n.a.		4.33	32.48	98.35	219	3	Mixed age
<2 µm	—	+++	o	—	+++	?	—	—	10	n.a.	n.a.		2.24	14.20	96.44	187	3	Mixed age
<0.2 µm	—	+++	—	—	++	—	—	FeS (o)	10	n.a.	n.a.		0.66	2.09	47.14	91	7	Fault reactivation (ca. 91 Ma)
GO-05-12																		
2–6 µm	—	++	+	—	++	+++	+	—	<10	n.a.	n.a.		3.49	22.52	98.12	190	3	Mixed age
<2 µm	—	+++	o	—	+	o	?	FeS (o)	<10	n.a.	n.a.		1.95	11.00	96.98	167	2	Mixed age
<0.2 µm	—	+++	—	—	+	—	?	FeS (+)	<10	n.a.	n.a.		0.59	2.30	26.30	117	9	Fault reactivation (ca. 117 Ma)

(Continues)

TABLE 1 (Continued)

Sample / Size fraction[a]	I/M	I/S	Kfs	Am	Chl	Qtz	Pl	Others	% Illite in I/S	KI_a	KI_g	KI zone	K_2O (wt. %)	$^{40}Ar^{*d}$ (nl/g) STP	$^{40}Ar^*$ (%)	Age (Ma)	$\pm2\sigma$ (Ma)	Interpretation[e]
GO-06-12																		
2–6 μm	?	++	+	—	+++	+	+	—	10–20	n.a.	n.a.		5.64	17.03	91.07	91	1	Uncertain intrepretation
2–6 μm/2													5.64	16.98	65.05	91	2	Uncertain intrepretation
<2 μm	—	+++	?	—	+++	o	o	—	10	n.a.	n.a.		1.69	10.52	96.06	183	3	Mixed age
<0.2 μm	—	+++	—	—	++	—	—	FeS (o)	10–20	n.a.	n.a.		0.42	1.98	40.37	141	13	Fault activity (ca. 151 Ma)
<0.2 μm/2													0.42	2.27	59.21	160	15	Fault activity (ca. 151 Ma)
GO-07-11																		
2–6 μm	+++	—	—	+	+	+	+	—	n.a.	0.43	0.42	Deep diagenetic zone	3.99	44.58	94.76	317	9	Mixed age
2–6 μm/2													3.99	45.19	95.18	320	11	Mixed age
<2 μm	+++	—	—	?	+	o	—	—	n.a.	0.55	0.62	Deep diagenetic zone	5.30	45.35	95.43	248	6	Fault activity (ca. 244 Ma)
<0.2 μm	+++	—	—	?	+	o	—	—	n.a.	0.58	0.61	Deep diagenetic zone	5.02	41.75	90.15	241	7	Fault activity (ca. 244 Ma)
GO-07-12																		
2–6 μm	+++	+	+	—	+	+	+	—	n.a.	0.44	0.44	Deep diagenetic zone	5.35	39.24	97.29	214	5	Mixed age
<2 μm	++	+++	+	—	++	+	—	—	10–20	0.60	0.57	Deep diagenetic zone	6.74	41.78	96.11	183	3	Mixed age
<0.2 μm	++	+++	o	—	++	—	—	—	20	0.77	0.66	Deep diagenetic zone	4.85	26.80	91.31	164	4	Approx. fault reactivation (ca. 164)
GO-08-12																		
2–6 μm	+++	++	—	—	+	o	o	—	<10	0.52	0.51	Deep diagenetic zone	6.05	54.55	97.31	260	3	Fault activity (ca. 262 Ma)
2–6 μm/2													6.05	55.61	97.21	265	3	Fault activity (ca. 262 Ma)
<2 μm	+	+++	—	—	+	—	—	—	<10	0.58	0.58	Deep diagenetic zone	2.77	23.17	93.83	242	5	Mixed age
<0.2 μm	o	+++	—	—	o	—	—	—	<10	0.77	0.80	Deep diagenetic zone	1.53	8.46	76.70	164	3	Fault reactivation (ca. 164 Ma)
GO-09-12																		
2–6 μm	+	++	—	—	+	—	—	Zeo (+++)	<10	n.a.	n.a.		1.34	6.79	58.69	151	3	Mixed age
<2 μm	++	+++	—	—	o	—	—	Zeo (++)	<10	0.47	0.42	Deep diagenetic zone	1.81	10.57	75.21	173	3	Fault activity (ca. 174 Ma)
<0.2 μm	o	+++	—	—	o	—	—	Zeo (+)	<10	1.31	1.33	Shallow diagenetic zone	1.96	11.65	69.48	176	3	Fault activity (ca. 174 Ma)

(Continues)

TABLE 1 (Continued)

Sample / Size fraction[a]	Mineralogy[b] I/M	I/S	Kfs	Am	Chl	Qtz	Pl	Others	% Illite in I/S	KI$_a$	KI$_g$	KI zone	K$_2$O (wt. %)	^{40}Ar*d (nl/g) STP	^{40}Ar* (%)	Age (Ma)	±2σ (Ma)	Interpretation[e]
<0.2 μm/2													1.96	11.59	73.59	175	3	Fault activity (ca. 174 Ma)
GO-10a-12																		
2–6 μm	++	+++	+	—	++	+	—	Zeo (+)	10–20	0.32	0.33	Low anchizone	3.32	19.18	83.81	171	5	Mixed age
<2 μm	+	+++	—	—	+	o	—	—	20–30	0.42	0.32	Low anchizone	4.22	28.02	88.41	195	3	Fault activity (ca. 192 Ma)
<0.2 μm	+	+++	—	—	+	o	—	—	30	0.45	0.43	Deep diagenetic zone	4.23	27.03	87.80	188	2	Fault activity (ca. 192 Ma)
GO-11-12																		
2–6 μm	++	+++	+	—	—	+	—	—	10	0.19	0.19	Epizone	5.77	43.00	99.05	217	6	Mixed age
<2 μm	+	+++	?	—	—	?	—	—	<10	n.a.	n.a.		4.63	29.72	96.31	189	6	Fault activity (ca. 189 Ma)
<0.2 μm	+	+++	?	—	—	?	—	—	<10	n.a.	n.a.		4.13	26.63	64.41	190	3	Fault activity (ca. 189 Ma)
GO-12-12																		
2–6 μm	o	+++	+	—	++	+	—	Ep (+)	20	0.46	0.41	Deep diagenetic zone	2.12	9.80	92.12	138	3	Mixed age
<2 μm	—	+++	—	—	++	?	—	Ep (o)	20–30	n.a.	n.a.		1.47	4.54	72.37	94	3	Mixed age
<0.2 μm	—	+++	—	—	++	—	—	—	20–30	n.a.	n.a.		0.94	1.77	43.48	57	2	Fault reactivation (ca. 57 Ma)
GO-13-12																		
2–6 μm	+	+++	—	+	+	—	—	Tlc (+)	<10	0.38	0.38	Low anchizone	3.58	44.80	93.86	351	4	Mixed age
<2 μm	o	+++	—	o	+	—	—	Tlc (++)	<10	n.a.	n.a.		2.04	22.39	91.17	312	3	Mixed age
<0.2 μm	?	+++	—	—	+	—	—	Tlc (++)	<10	n.a.	n.a.		1.03	9.55	78.63	268	7	Fault reactivation (ca. 268 Ma)
GO-14-12																		
2–6 μm	+++	—	—	—	++	+	+	FeS (o), Zeo (?)	n.a.	0.15	0.15	Epizone	6.38	69.87	97.82	311	4	Fault activity (ca. 311 Ma)
<2 μm	++	+++	—	—	++	—	o	FeS (+)	40–50	0.22	0.22	Epizone	4.87	42.67	90.51	253	5	Mixed age
<0.2 μm	+	+++	—	—	+	—	?	FeS (+++)	40–50	0.25	0.24	Epizone	3.18	18.58	75.36	172	2	Max. age reactivation (<172 Ma)
GO-15-12																		
2–6 μm	+++	—	+	+	++	+	+	—	n.a.	0.35	0.34	Low anchizone	5.19	57.98	90.04	317	4	Max. age fault activity (<317 Ma)
<2 μm	+++	—	?	o	+	o	o	—	n.a.	0.42	0.43	Deep diagenetic zone	6.83	66.35	85.66	279	3	Mixed age

TABLE 1 (Continued)

Sample / Size fraction[a]	Mineralogy[b] I/M	I/S	Kfs	Am	Chl	Qtz	Pl	Others	% Illite in I/S	Illite crystallinity[c] KI$_a$	KI$_g$	KI zone	K$_2$O (wt. %)	^{40}Ar*[d] (nl/g) STP	^{40}Ar* (%)	Age (Ma)	±2σ (Ma)	Interpretation[e]
<0.2 μm	+++	—	—	—	+	?	—	—	n.a.	0.61	0.56	Deep diagenetic zone	6.58	46.97	82.44	209	3	Fault reactivation (ca. 209 Ma)
BG-129a																		
2–6 μm	—	+++	+	—	++	+	—	Ep (o)	20–30	n.a.	n.a.		2.99	14.99	89.51	149	4	Fault activity (ca. 145 Ma)
<2 μm	o	+++	o	—	++	—	—	Ep (o)	30	0.31	0.28	High anchizone	2.30	11.10	77.54	144	2	Fault activity (ca. 145 Ma)
<0.2 μm	o	+++	—	—	+	—	—	—	30	n.a.	0.29	High anchizone	1.57	3.30	55.77	64	1	Fault reactivation (ca. 64 Ma)
BG-129b																		
2–6 μm	—	++	++	—	+	++	—	Ep (+)	n.a.	n.a.	n.a.		5.39	35.06	98.74	191	3	Mixed age
<2 μm	o	+++	o	—	+	—	—	Ep (o)	10–20	0.24	0.24	Epizone	4.09	19.55	94.86	142	2	Fault activity (ca. 145 Ma)?
<0.2 μm	o	+++	o	—	+	—	—	—	n.a.	0.36	0.23	Epizone-high anchizone	2.43	8.58	86.34	106	2	Mixed age

Abbreviations: Chl, chlorite; Ep, epidote; FeS, Fe-sulfide; I/M, illite/muscovite; I/S, illite/smectite; Kfs, K-feldspar; Minerals: Am, amphibole; Pl, plagioclase; Qtz, quartz; Tlc, talc; Zeo – zeolite.

[a]/2 after grain size fraction marks duplicate analyses.

[b]+++ main component, ++ significant component, + minor component, o traces, ? uncertain, — not identified.

[c]Kübler Index in Δ°2θ, KI$_a$ - air-dried, KI$_g$ - ethylene glycol-solvated.

[d]Ar* - radiogenic argon, STP - standard temperature and pressure conditions.

[e]See supplementary material, Chapter 3 for a full discussion of each fault.

size fractions overlap in age, forming an age plateau, this age is interpreted to represent extensive illite crystallisation corresponding to a significant event in the fault's history.

4 | SAMPLES, RESULTS AND INTERPRETATIONS

The ages obtained for each of the three grain-size fractions (2–6, <2 and <0.2 μm) are presented in Table 1. Ages within the entire dataset range from Late Devonian (374 Ma) to Paleocene (57 Ma). The spread of ages within individual samples varies from 24 to 139 Ma with an average of 80 Ma, and ages generally decrease with grain-size (Figure 5). The results for each sample are interpreted and presented in full in the supporting information, as sorted into subareas A-F (Figure 5). Below we present a short summary of each subarea, before considering the data collectively in the context of the regional tectonic evolution.

4.1 | Gurskøya – Austefjorden (Subarea A)

Subarea A encompasses samples GO-07-11 (Gurskøya), GO-11-12, GO-09-12 and GO-10a-12 (Austefjorden). The three samples from Austefjorden all document growth of illite during fault activity in the Early Jurassic, from ~192 to 174 Ma (Figure 5a). The illite in sample GO-07-11, moreover, documents an earlier period of fault activity in the Middle Triassic (~244 Ma). None of these samples preserve clear evidence of either earlier fault activity or later fault reactivation. One of the samples from Austefjorden (GO-11-12) and the sample from Gurskøya (GO-07-11) contain an older generation of higher-temperature illite or muscovite. Although this might suggest an earlier period of fault activity, it could equally well be explained by minor amounts of inherited muscovite from the host rock. The only evidence of later (post-Early Jurassic) reactivation might be zeolite present in samples GO-09-12 and GO-10a-12, but we consider this to be highly speculative.
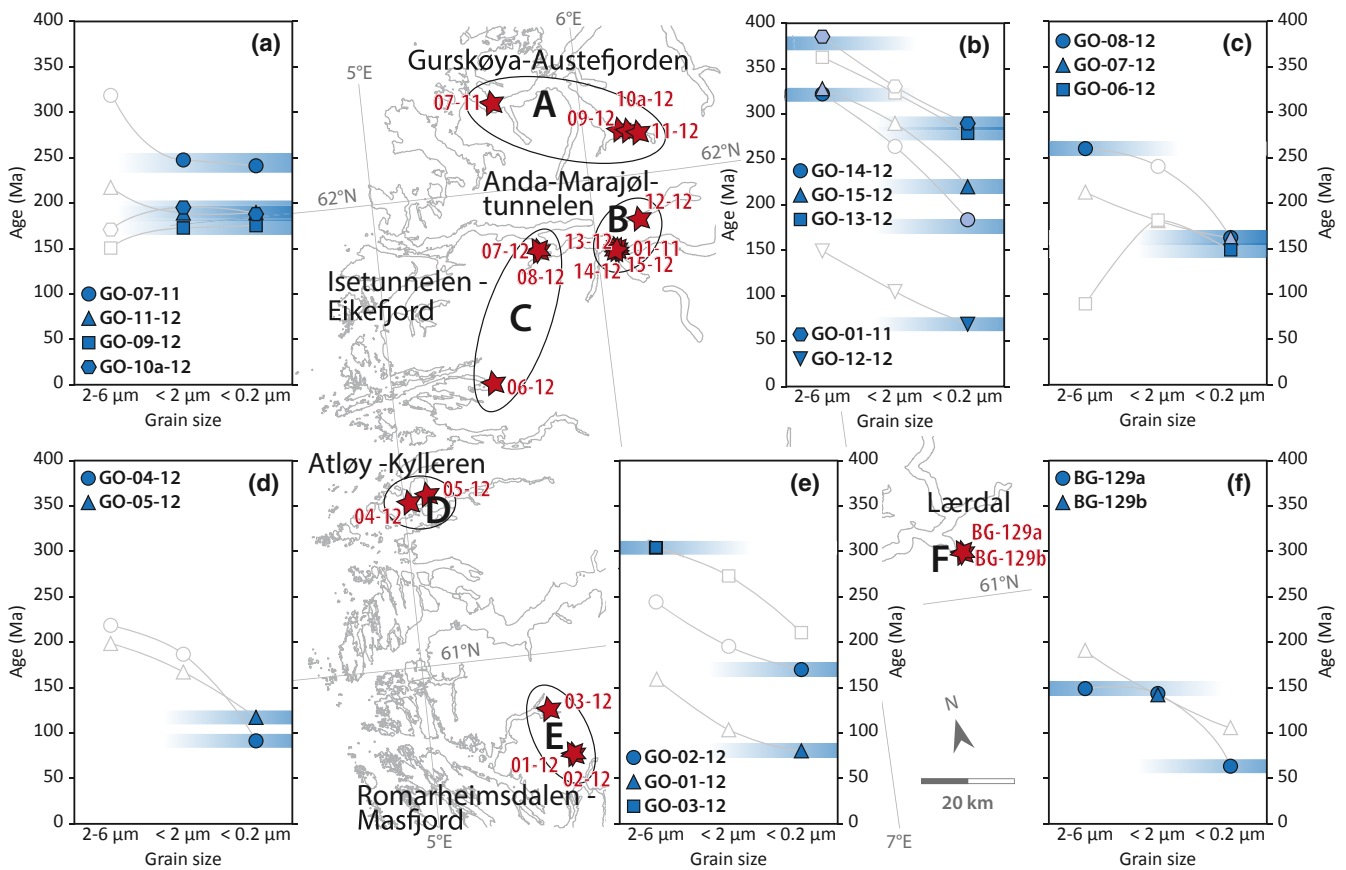
FIGURE 5 Age versus grain size plots for dated faults from subareas (a-f). Dark blue symbols mark ages interpreted to date fault activity; light blue symbols represent ages that are close to the age of fault activity (max./min. ages for fault activity) and empty symbols are ages that are interpreted as mixed ages of uncertain geological significance. Blue bars mark interpreted periods of fault activity

4.2 | Anda and Marajøltunnelen (Subarea B)

Subarea B samples are GO-14-12, GO-15-12, GO-13-12, GO-01-11 (all from Anda) and GO-12-12 (Marajøltunnelen). The four samples from Anda yielded some of the oldest illite ages in our dataset and document illite growth in faults as early as Late Devonian (GO-01-11, possibly also GO-13-11) and late Carboniferous (GO-14-12 and GO-15-12) times (Figure 5b). All four faults were reactivated in the late Paleozoic-Mesozoic, i.e. in the middle Permian (GO-01-11 and GO-13-12), Late Triassic (GO-15-12) and Middle Jurassic (GO-14-12). The fault close to Marajøltunnelen (GO-12-12), moreover, yielded some of the youngest illite ages, indicating fault reactivation in the late Paleocene. Earlier activity along this fault is suggested by the older ages of the coarse and medium grain size fractions but could not be reliably constrained.

4.3 | Isetunnelen and Eikefjord (Subarea C)

Subarea C includes samples GO-08-12 and GO-07-12 (Isetunnelen), and GO-06-12 (Eikefjord). All three faults were active in the Middle-Late Jurassic (~164–151 Ma; Figure 5c). An earlier, late Permian period of fault activity is documented by the coarse fraction of sample GO-08-12. Sample GO-07-12 also shows evidence of earlier (Triassic?) illite growth that could, however, not be precisely constrained.

4.4 | Dalsfjord Fault: Atløy and Kylleren (Subarea D)

Samples GO-04-12 (Atløy) and GO-05-12 (Kylleren) sample fault gouge along the Dalsfjord Fault. Both gouge samples record Cretaceous fault activity (~117–91 Ma; Figure 5d). The older ages of the medium and coarse grain size fractions, though mixed ages of uncertain significance, suggest Cretaceous reactivation of an older structure. Field evidence also points to a multiply reactivated fault, with several generations of ductile-brittle fault rocks cut by the youngest, gouge-bearing fault. GO-04-12 was sampled at the location described by Eide et al. (1997), who obtained an age of ~260–250 Ma for a green breccia/cataclasite, an age younger than 163 Ma for a red breccia/cataclasite and assumed an age younger than 96 Ma for the fault gouge at the same locality. The latter is confirmed by our Late Cretaceous age of 91 Ma.

4.5 | Romarheimsdalen and Masfjorden (Subarea E)

Subarea E samples are GO-02-12 and GO-01-12 (Romarheimsdalen), and GO-03-12 (Matre). All three faults preserve evidence of an earlier period of fault activity and a later reactivation. In the two faults from Romarheimsdalen, the older activity is suggested by the older ages of the coarser grain size fractions but could not be reliably constrained. The faults were reactivated in the Middle Jurassic (~170 Ma) and Late Cretaceous (~80 Ma), respectively (Figure 5e). For sample GO-03-12 from Matre, moreover, and early period of late Carboniferous (~304 Ma) fault activity is well preserved, and the age of reactivation can only vaguely be constrained to be Late Triassic or younger («211 Ma).

4.6 | Lærdal-Gjende Fault (Subarea F)

Two samples, BG-129a and b, were collected from the Lærdal-Gjende Fault in Lærdal. The coarse and medium fractions of BG-129a and the medium fraction of the sample BG-129b indicate a latest Jurassic-earliest Cretaceous period of significant, fully brittle fault activity along the Lærdal-Gjende Fault. In addition, the fine fraction from BG-129b suggests the second period of fault reactivation in the early Paleogene (Figure 5f). This confirms late Jurassic-early Cretaceous fault activity previously 'dated' at the same outcrop by paleomagnetic methods (Andersen et al., 1999). These results are also broadly similar to K-Ar illite results from the same locality presented by Tartaglia et al. (2020), who report a Jurassic age cluster and also a number of reactivation ages from ca. 120 to 60 Ma.

4.7 | General distribution of fault gouge ages and fault orientations

We now combine the new ages presented above with published ages south of our study area, primarily those presented by Ksienzyk et al. (2016) but also some ages farther south presented by Scheiber and Viola (2018), Scheiber et al. (2019), Fossen et al. (2016) and Viola et al. (2016; Figure 1). Considering only ages that are interpreted to date or closely date faulting, we see a range in ages from Late Devonian to early Paleogene (Figure 6). This distribution shows clear Permian and Jurassic peaks that roughly coincide with the onset of the two main rift phases in the northern North Sea rift, as discussed below.

There is no clear systematic variation in the ages with respect to geographic distribution (Figure 4). From our new data (Figure 5) we see young ages close to the coast (groups D and E) and far inland (group F). The largest spread in ages is found in Group B in the detachment zone east of the Devonian Hornelen basin (Figure 2). In general, our data suggest that faults formed and reactivated widely within the entire study area during the Late Devonian-Paleocene time period. The data presented by Ksienzyk et al. (2016) from the
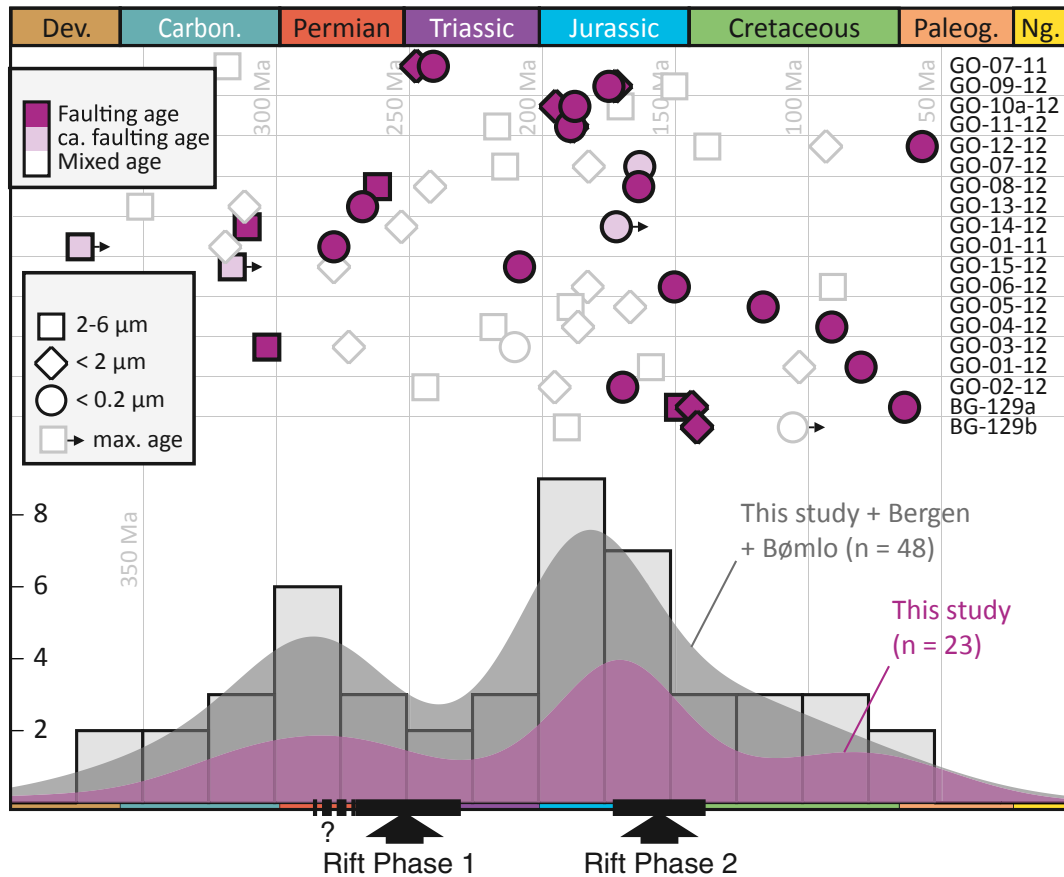
FIGURE 6 Fault gouge grain size fraction ages, divided into three categories: (1) age of fault activity, no or only minor contamination. (2) Approximate age of fault activity – generally dates fault activity but affected by minor contamination with another age component. We still consider this age geologically meaningful, since it can provide a maximum or minimum age of fault activity. (3) Mixed age – different age components contribute, and the age has no geological significance. Mixed ages are not used for interpretations. The histogram and kernel density estimates (KDEs) were plotted with IsoplotR (Vermeesch, 2018) using a kernel bandwidth of 25 and are based on interpreted fault activity ages from Table S2. If several grain size fractions or samples from a given fault date the same period of fault activity, the mean age is included as the interpreted fault activity age for the respective fault. Violet KDE: this study; gray KDE + histogram: combined data from this study, Ksienzyk et al. (2016), Viola et al. (2016), Scheiber and Viola (2018) and Scheiber et al. (2019)

Bergen area as well as those reported by Viola et al. (2016), Scheiber and Viola (2018) and Scheiber et al. (2019) from farther south are consistent with this impression.

When considering the ages with respect to fault orientation (Figure 7a), we see some correlation between age distribution and fault orientation for the 48 dated faults in W Norway. We show this by defining three groups of strike orientation; NW-NNW, N-NNE and NE-E. Keeping in mind that our current dataset is limited, we note that the age distributions for these different orientation groups (Figure 7b-d) suggest that all groups contain relatively old (>300 Ma) ages that clearly predate the North Sea rift. All groups show a strong Jurassic (200–145 Ma) signal, whereas the Permian peak is best developed for NW-NNW trending faults. Interestingly, the NNW-trending Austefjord Fault (AF in Figure 1) that hosts Permian dikes west of Bergen (Løvlie & Mitchell, 1982) falls within the sector showing a strong Permian signature. This observation supports the general assumption that coast (and
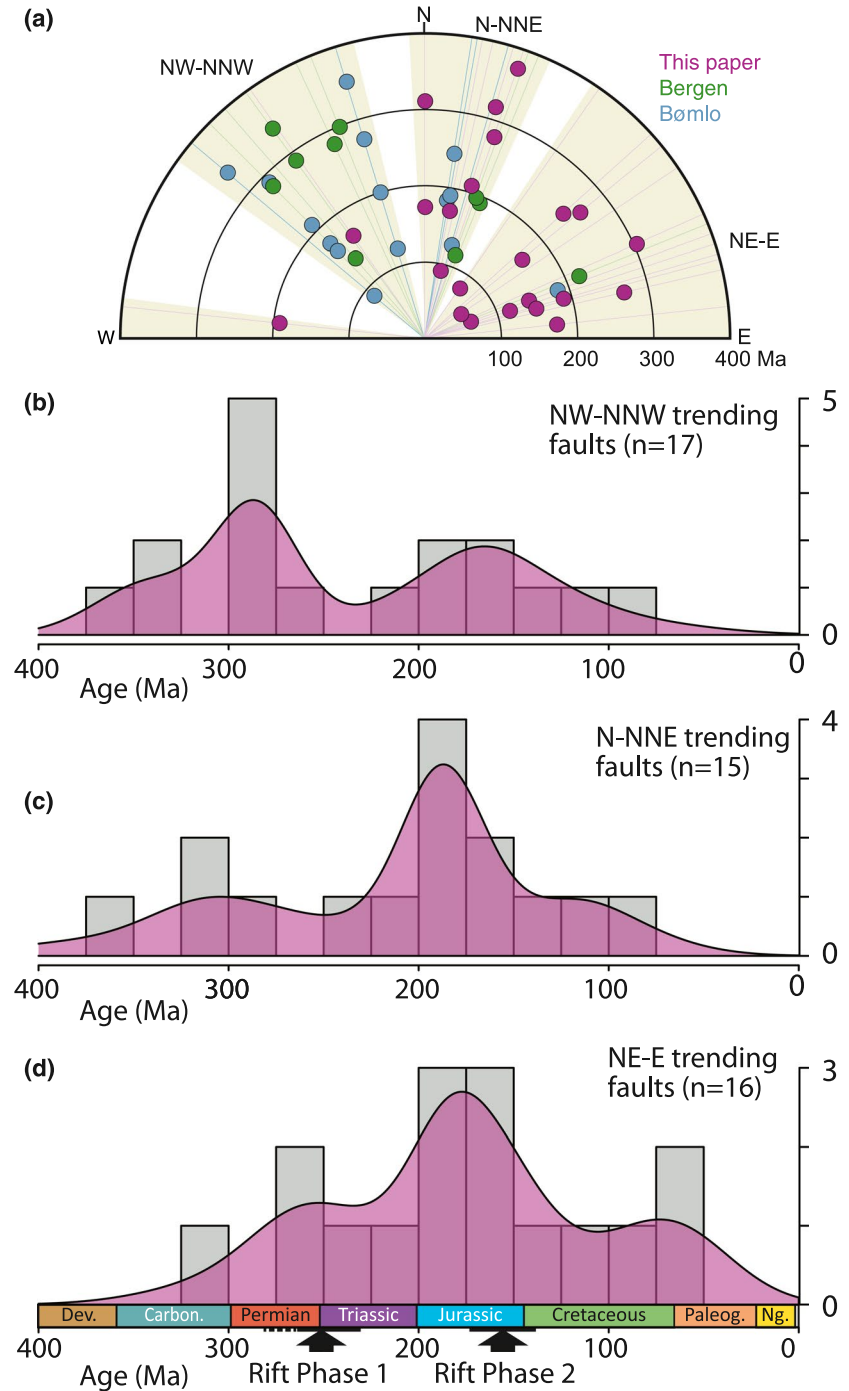
rift) parallel faults formed or reactivated during the Permo-Triassic phase of rifting (Fossen, 1998).

5 | DISCUSSION

5.1 | Deep post-Caledonian fault gouge formation

Our oldest fault activity age is Late Devonian (374 Ma) and occurs in the NSDZ east of the Hornelen basin (sample GO-01-11). This is located in the root zone of the Caledonian hinterland – a region that underwent rapid exhumation and cooling following the ca. 425–405 Ma Caledonian continental subduction. A muscovite ^{40}Ar/^{39}Ar plateau age of ca. 398 Ma from this locality (Young et al., 2011) probably dates Early Devonian cooling through 400–450°C (13–15 km crustal depth). K-feldspar ^{40}Ar/^{39}Ar data from this part of the study

area region suggest cooling through ~400°C between 390 and 330 Ma and through 200°C (~6 km) around 310–230 Ma (Walsh et al., 2013). Zircon apatite ages of around 230 Ma (200–250°C) were reported by Templeton (2015) for the Hornelen area. Based on these constraints, the 374 Ma illite age must record early brittle deformation of these rocks as they passed through the plastic-brittle transition zone. These constraints imply that faulting occurred at 8–10 km depth, producing mechanically weak incohesive fault gouge deep in the strongest part of the crust. If widespread, such weak faults would significantly weaken the crust before rifting and

be prone to reactivation during rift initiation. Other than the Late Devonian age presented here, early Carboniferous brittle fault activity has so far been tentatively documented in one fault from the Bergen area (Ksienzyk et al., 2016) and the Goddo fault (Viola et al., 2016), and is convincingly constrained by multiple K-Ar dates from another fault from the Bømlo area (Scheiber et al., 2019). Though the number of faults with such an old signature is small in the presently available dataset from SW Norway, it is possible that similar evidence of early brittle faulting in other faults may have been erased by later tectono-diagenetic processes.

5.2 | Rift-related faulting

The older of the two prominent age-peaks in our dataset ranges from late Carboniferous to Early Triassic, which is exactly the time span of rifting in the Oslo Rift (Larsen et al., 2008). The Oslo Rift is part of the Rotliegendes basin system in northern Europe and developed in response to the late Variscan orogeny during dextral slip on the Tornquist Zone (Figure 1; Heeremans & Faleide, 2004; Larsen et al., 2008). In the Oslo and southern North Sea rifts, the initiation of this event is marked by a magmatic phase at around 300 Ma, followed by half-graben development and synrift sedimentation. Late Carboniferous-Permian activity appears to be more limited in the northern North Sea Rift, which along the SW Norwegian margin up to 61°N is dominated by Early Triassic fault-controlled sedimentation (e.g. Øygarden Fault System; Figure 1). Permian synrift deposits occur in mostly undrilled hanging-wall parts of major half-grabens but are not dated. Hence, exactly when the Permo-Triassic rift phase initiated is still somewhat enigmatic, as indicated by the dashed line and question mark at the bottom of Figure 6. What seems clear is that the peak of this rift phase offshore in terms of fault movements and basin growth occurred in the Early Triassic (Heeremans & Faleide, 2004).

North of 61°N, the crystalline basement of the Måløy Slope (Figure 1) is directly overlain by Jurassic and younger sediments (Figure 3; Færseth et al., 1995), whereas most of the Permo-Triassic strain is transferred westward to the Tampen area and the East Shetland Basin. With a prominent Permian onshore fault signature also north of 61°N, we would expect faults of this age also offshore, but only with offsets that are too small to be detected from even modern 3-D seismic data (Figure 3) and too small to create any Permo-Triassic half-graben basin(s).

Independent onshore indications of Permian tectonism include a thick greenish cataclasite of the Lærdal-Gjende fault (Figure 1) which at locality BG-129 carries a mid-late Permian magnetic signature (Andersen et al., 1999). A similar (~260 Ma) paleomagnetic age was obtained from locality GO-04-12 (Dalsfjord Fault Eide et al., 1997; Torsvik et al., 1992). Both faults were later reactivated in the late Jurassic-early Cretaceous (Andersen et al., 1999; Eide et al., 1997) and Cretaceous-early Paleogene (this study). A Permian age was also obtained by $^{40}Ar/^{39}Ar$ dating of potassium feldspar altered by fault-related fluids in fractured basement gneisses west of Bergen (Fossen et al., 2016).

Rift-parallel Permian and Triassic dikes occur in the coastal areas of the studied rift margin (Færseth et al., 1976; Torsvik et al., 1997), consistent with E-W extension (Fossen, 1998). Dikes intruded at 260–250 and 230–220 Ma (Fossen & Dunlap, 1999), and are located along coast-parallel fault zones of likely Permian age (Fossen, 1998). In

summary, abundant evidence now exists for Permian tectonic activity onshore SW Norway, even north of 61°N where near-shore Permian faulting appears to mainly be of subseismic (small-scale) character (Færseth et al., 1995).

Onshore, the Triassic period as a whole seems to have been rather quiet, whereas the Jurassic has a strong signature (Figure 6). In the North Sea, the second phase of rifting is Middle Jurassic to Early Cretaceous (ca. 170–140 Ma). However, there is also evidence of scattered Triassic-early Jurassic interrift fault activity (Deng et al., 2017; Ravnås et al., 2000), as reflected by the onshore age distribution reported here (Figure 6). Faulted Oxfordian sediments preserved in the Bjorøy tunnel near Bergen represent additional evidence of Late Jurassic to Early Cretaceous fault activity involving >100 m of offset (Fossen et al., 1997).

Besides the Lærdal-Gjende and Dalsfjord faults, the Bortnen Fault northeast of the Hornelen Basin (Figures 1 and 2) represents a third major fault in the area that was dated. This fault represents one of the ENE-trending major faults in the northern part that affect the Devonian basins and the underlying units. Sample GO-12-12, from a NE-SW trending fault near and subparallel to the Bortnen Fault (Figures 1 and 2) yielded the youngest fault activity age (57 Ma) reported from SW Norway to date.

The finding that around 70% of the available illite ages coincide in time with the period of North Sea rifting (Permian-Early Cretaceous; Figure 6) demonstrates that the onshore basement was significantly influenced by rift-related faulting. This conclusion is corroborated by the gradual increase in fault density westwards towards the main rift-bounding faults, over a distance of ~100 km (Figure 4).

5.3 | Implications for rift evolution

The basement exposed onshore West Norway contains Devonian shear zones that affected the evolution of the northern North Sea rift (Fossen et al., 2016; Fazlikhani et al., 2017; Wiest et al., 2020). Their reactivation during rifting is consistent with the Permian-Early Cretaceous ages obtained from brittle faults developed along these shear zones (Lærdal-Gjende Fault, Bortnen Fault, Dalsfjord Fault; Figure 2). In addition, the results presented here show that the Lower Paleozoic and older onshore, and probably also offshore, basement was affected by post-Caledonian brittle deformation that weakened the brittle crust prior to rift initiation. Similarly, post-Caledonian brittle faults onshore and offshore Scotland and in the West Orkney Basin are widespread and predominantly Permo-Triassic in age (Roberts & Holdsworth, 1999; Wilson et al., 2010), suggesting that early rift faults also formed far into the western North Sea rift shoulder.

The onshore Permian and Jurassic fault activity peaks match or immediately predate the initial stages rather than the climaxes of the two offshore rift phases (Figure 6). As discussed above, the Permo-Triassic rift phase peaked in the Early Triassic in the main rift, although our data show that related onshore tectonism peaked already in the Permian and that it was distributed over a region that extends >100 km into the Norwegian mainland (future rift shoulder; Figure 8a). Only towards the end of the Permian or at the dawn of the Triassic did extension localise to define the North Sea rift proper, bounded by faults that accumulated kilometre-size early Triassic offsets and thick synrift half-graben deposits (Figures 1 and 8b; Færseth, 1996; Roberts et al., 1995). Similarly, the Jurassic onshore fault activity ages peak before the offshore late Jurassic rifting climax (Figure 6), indicating that also the Jurassic rift event started out much wider than the rift proper as a prelude to rifting per-se, again extending at least 100 km into the Norwegian rift shoulder. At this time a Permo-Triassic rift was already established with major bounding faults (the Øygarden Fault System; Figure 1), and it is not clear why the early Phase 2 extension did not

immediately localise to the large Phase 1 rift faults. Perhaps it relates to the onshore Phase 1 faults having significantly weakened the shoulder basement, or that the lithosphere was thermally softened over a wide region as Phase 2 initiated.

The effect of embryonic rifting >100 km into the rift shoulder, i.e. outside of the main rift, has to our knowledge not been documented before. Strain localisation *within* already well-established rifts are well known, for example from the East African, Suez and Rio Grande rifts (Bosworth, 1995; Cowie et al., 2000, 2005; Minor et al., 2013) and (oblique) physical and numerical experiments (Agostini et al., 2009; Duclaux et al., 2020). Within the North Sea rift, Cowie et al. (2005) documented that extension further localised to the ~50 km wide Viking Graben during the last part of the second North Sea rift phase. Together with our documentation of brittle faulting >100 km into the rift shoulder at the early stages of both North Sea rift phases, the history and amount of strain localisation is remarkable. Our new data indicate that (a) the region affected by faulting during early-stage rifting was far wider than previously assumed, probably several hundred kilometres if we make the likely assumption
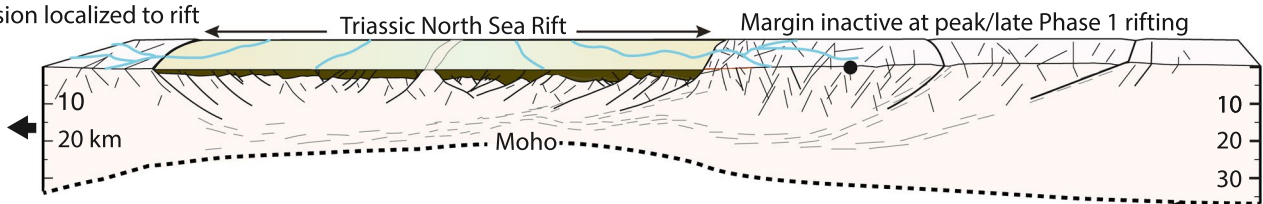

(a) Incipient rifting (Early-Mid Permian): Widely distributed faulting
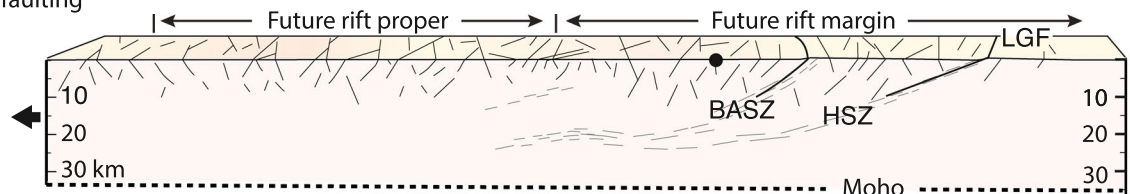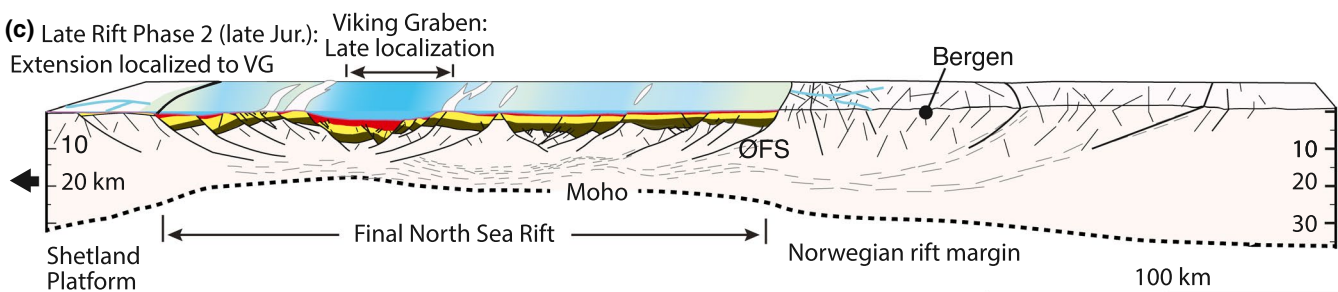
(b) Late Rift Phase 1 (Triassic): Extension localized to rift

(c) Late Rift Phase 2 (late Jur.): Extension localized to VG

FIGURE 8 Simplified illustration of the tectonic model presented in this work. (a) Initial rift stage with widely distributed small-scale faulting that includes a combination of reactivation of prerift structures and the formation of new faults. (b) Mature rift situation, where the rift with its large normal faults has developed within a restricted part of the initial region of extension. (c) Final localisation of strain to the central part of the rift (Viking Graben for the second North Sea rift phase). Yellow layer represents the interrift sequence deposited between the two North Sea rift phases. See caption to Figure 1 for abbreviations

that it also affected the North Sea rift itself, and (b) the narrowing of the region of active extension and associated strain localisation was more pronounced than previously realised, eventually down to a 50 km wide central rift (Viking Graben; Figure 8c). We consider it likely that widespread early-stage rift faulting extending far into the rift shoulder may apply to many other rifts globally. In many cases, this can only be investigated by means of work-intensive fault dating utilising relatively modern methodology. Our work demonstrates how K-Ar dating can be a useful way of evaluating the impact of rifting on rift shoulders where stratigraphic constraints are lacking.

DATA AVAILABILITY STATEMENT

The data that form the basis of this work are available in the Supporting Information.

ORCID

Haakon Fossen (iD) https://orcid.org/0000-0002-8091-5643
Atle Rotevatn (iD) https://orcid.org/0000-0002-8413-3294

REFERENCES

Agostini, A., Corti, G., Zeoli, A., & Mulugeta, G. (2009). Evolution, pattern, and partitioning of deformation during oblique continental rifting: Inferences from lithospheric-scale centrifuge models. *Geochemistry, Geophysics, Geosystems*, *10*. https://doi.org/10.1029/2009gc002676

Andersen, T. B., Torsvik, T. H., Eide, E. A., Osmundsen, P. T., & Faleide, J. I. (1999). Permian and Mesozoic extensional faulting within the Caledonides of central south Norway. *Journal of the Geological Society*, *156*, 1073–1080. https://doi.org/10.1144/gsjgs.156.6.1073

Arnaud, N. O., & Eide, E. A. (2000). Brecciation-related argon redistribution in alkali feldspars: an in naturo crushing study. *Geochimica Et Cosmochimica Acta*, *64*, 3201–3215. https://doi.org/10.1016/s0016-7037(00)00411-7

Bell, R. E., Jackson, C. A. L., Whipp, P. S., & Clements, B. (2014). Strain migration during multiphase extension: Observations from the northern North Sea. *Tectonics*, *33*, 1936–1963. https://doi.org/10.1002/2014TC003551

Bense, F. A., Wemmer, K., Löbens, S., & Siegesmund, S. (2014). Fault gouge analyses: K-Ar illite dating, clay mineralogy and tectonic significance – a study from the Sierras Pampeanas, Argentina. *International Journal of Earth Sciences*, *103*, 189–218. https://doi.org/10.1007/s00531-013-0956-7

Berry, H. N., Lux, D. R., Andresen, A., & Andersen, T. B. (1995). Progressive exhumation during orogenic collapse as indicated by 40Ar/39Ar cooling ages from different structural levels, southwest Norway (Abstract). *Geonytt*, *22*, 20–21.

Bosworth, W. (1995). A high-strain rift model for the southern Gulf of Suez (Egypt). *Geological Society Special Publication*, *80*, 75–102. https://doi.org/10.1144/GSL.SP.1995.080.01.04

Boundy, T. M., Essene, E. J., Hall, C. M., Austrheim, H., & Halliday, A. N. (1996). Rapid exhumation of lower crust during continent-continent collision and late extension: evidence from 40Ar-39Ar incremental heating of hornblendes and muscovites, caledonian orogen, western Norway. *Geological Society of America Bulletin*, *108*, 1425–1437.

Braathen, A. (1999). Kinematics of post-Caledonian polyphase brittle faulting in the Sunnfjord region, western Norway. *Tectonophysics*, *302*, 99–121. https://doi.org/10.1016/S0040-1951(98)00281-9

Chauvet, A., & Dallmeyer, R. D. (1992). 40Ar/39Ar mineral dates related to Devonian extension in the southwestern Scandinavian Caledonides. *Tectonophysics*, *210*, 155–177.

Cowie, P., Gupta, S., & Dawers, N. H. (2000). Implications of fault array evolution for synrift depocentre development: Insights from a numerical fault growth model. *Basin Research*, *12*, 241–261. https://doi.org/10.1111/j.1365-2117.2000.00126.x

Cowie, P., Underhill, J. R., Behn, M. D., Lin, J., & Gill, C. E. (2005). Spatio-temporal evolution of strain accumulation derived from multi-scale observations of Late Jurassic rifting in the northern North Sea: A critical test of models for lithospheric extension. *Earth and Planetary Science Letters*, *234*, 401–419. https://doi.org/10.1016/j.epsl.2005.01.039

Deng, C., Fossen, H., Gawthorpe, R. L., Rotevatn, A., Jackson, C. A. L., & FazliKhani, H. (2017). Influence of fault reactivation during multiphase rifting: The Oseberg area, northern North Sea rift. *Marine and Petroleum Geology*, *86*, 1252–1272. https://doi.org/10.1016/j.jsg.2017.11.005

Doré, A. G., Lundin, E. R., Jensen, L. N., Birkeland, Ø., Eliassen, P. E., & Fichler, C. (1999). Principal tectonic events in the evolution of the northwest Eurpoean Atlantic margin. In: A. J. Fleet, & S. A. R. Boldy (Eds.), *Petroleum Geology of Northwest Europe* (pp. 41–61). Proceedings of the 5th Conference. Geological Society.

Duclaux, G., Huismans, R. S., & May, D. A. (2020). Rotation, narrowing, and preferential reactivation of brittle structures during oblique rifting. *Earth and Planetary Science Letters*, *531*, 115952. https://doi.org/10.1016/j.epsl.2019.115952

Dunlap, W. J., & Fossen, H. (1998). Early Paleozoic orogenic collapse, tectonic stability, and late Paleozoic continental rifting revealed through thermochronology of K-feldspars, southern Norway. *Tectonics*, *17*, 604–620.

Eide, E. A., Torsvik, T. H., & Andersen, T. B. (1997). Absolute dating of brittle fault movements: Late Permian and late Jurassic extensional fault breccias in western Norway. *Terra Nova*, *9*, 135–139.

Eide, E., Torsvik, T. H., Andersen, T. B., & Arnaud, N. O. (1999). Early Carboniferous unroofing in western Norway: a tale of alkali feldspar thermochronology. *The Journal of Geology*, *107*, 353–374.

Færseth, R. B. (1996). Interaction of Permo-Triassic and Jurassic extensional fault-blocks during the development of the northern North Sea. *Journal of the Geological Society*, *153*, 931–944.

Færseth, R. B., Gabrielsen, R. H., & Hurich, C. A. (1995). Influence of basement in structuring of the North Sea basin, offshore southwest Norway. *Norsk Geologisk Tidsskrift*, *75*, 105–119.

Færseth, R. B., Macintyre, R. M., & Naterstad, J. (1976). Mesozoic alkaline dykes in the Sunnhordland region, western Norway: Ages, geochemistry and regional significance. *Lithos*, *9*, 331–345.

Fazlikhani, H., Fossen, H., Gawthorpe, R. L., Faleide, J. I., & Bell, R. E. (2017). Basement structure and its influence on the structural configuration of the northern North Sea rift. *Tectonics*, *36*, 1151–1177.

Fossen, H. (1998). Advances in understanding the post-Caledonian structural evolution of the Bergen area. *West Norway: Norsk Geologisk Tidsskrift*, *78*, 33–46.

Fossen, H. (2010). Extensional tectonics in the North Atlantic Caledonides: A regional view. *Geological Society Special Publication*, *335*, 767–793.

Fossen, H., & Dallmeyer, R. D. (1998). 40Ar/39Ar muscovite dates from the nappe region of southwestern Norway: Dating extensional deformation in the Scandinavian Caledonides. *Tectonophysics*, *285*, 119–133.

Fossen, H., & Dunlap, W. J. (1998). Timing and kinematics of caledonian thrusting and extensional collapse, southern Norway: evidence from 40Ar/39Ar thermochronology. *Journal of Structural Geology*, *20*, 765–781.

Fossen, H., & Dunlap, W. J. (1999). On the age and tectonic significance of Permo-Triassic dikes in the Bergen-Sunnhordland region, southwestern Norway. *Norsk Geologisk Tidsskrift*, *79*, 169–178.

Fossen, H., & Dunlap, W. J. (2006). Age constraints on the late Caledonian deformation in the Major Bergen Arc, SW Norway. *Norwegian Journal of Geology*, *86*, 59–70.

Fossen, H., Khani, H. F., Faleide, J. I., Ksienzyk, A. K., & Dunlap, W. J. (2016). Post-Caledonian extension in the West Norway-northern North Sea region: The role of structural inheritance. *Geological Society Special Publication*, *439*, 465–486. https://doi.org/10.1144/sp439.6

Fossen, H., Mangerud, G., Hesthammer, J., Bugge, T., & Gabrielsen, R. H. (1997). The Bjorøy Formation: A newly discovered occurrence of Jurassic sediments in the Bergen Arc System. *Norsk Geologisk Tidsskrift*, *77*, 269–287.

Gabrielsen, R. H., Braathen, A., Dehls, J., & Roberts, D. (2002). Tectonic lineaments of Norway. *Norwegian Journal of Geology*, *82*, 153–174.

Haines, S. H., & van der Pluijm, B. A. (2008). Clay quantification and Ar–Ar dating of synthetic and natural gouge: Application to the Miocene Sierra Mazatán detachment fault, Sonora, Mexico. *Journal of Structural Geology*, *30*, 525–538. https://doi.org/10.1016/j.jsg.2007.11.012

Heeremans, M., & Faleide, J. I. (2004). Late Carboniferous-Permian tectonics and magmatic activity in the Skagerrak. *Kattegat and the North Sea: Geological Society Special Publication*, *223*, 157–176.

Ksienzyk, A. K., Wemmer, K., Jacobs, J., Fossen, H., Schomberg, A. C., Süssenberger, A., Lünsdorf, N. K., & Bastesen, E. (2016). Post-Caledonian brittle deformation in the Bergen area, West Norway: Results from K-Ar illite fault gouge dating. *Norwegian Journal of Geology*, *96*, 275–299. https://doi.org/10.17850/njg96-3-06

Larsen, B. T., Olaussen, S., Sundvoll, B., & Heeremans, M. (2008). The Permo-Carboniferous Oslo Rfit through six stages and 65 million years. *Episodes*, *31*, 52–58.

Larsen, Ø., Fossen, H., Langeland, K., & Pedersen, R. B. (2003). Kinematics and timing of polyphase post-Caledonian deformation in the Bergen area, SW Norway. *Nowegian Journal of Geology*, *83*, 149–165.

Löbens, S., Bense, F. A., Wemmer, K., Dunkl, I., Costa, C. H., Layer, P., & Siegesmund, S. (2011). Exhumation and uplift of the Sierras Pampeanas: Preliminary implications from K-Ar fault gouge dating and low-T thermochronology in the Sierra de Comechingones (Argentina). *International Journal of Earth Sciences*, *100*, 671–694. https://doi.org/10.1007/s00531-010-0608-0

Løvlie, R., & Mitchell, J. G. (1982). Complete remagnetization of some Permian dykes from western Norway induced during burial/uplift. *Physics of the Earth and Planetary Interiors*, *30*, 415–421.

Minor, S. A., Hudson, M. R., Caine, J. S., & Thompson, R. A. (2013). Oblique transfer of extensional strain between basins of the middle Rio Grande rift, New Mexico: Fault kinematic and paleostress constraints. *Geological Society of America Special Paper*, *494*, 345–382. https://doi.org/10.1130/2013.2494(14)

Odinsen, T., Reemst, P., Beek, P. V. D., Faleide, J. I., & Gabrielsen, R. H. (2000). Permo-Triassic and Jurassic extension in the northern North Sea: Results from tectonostratigraphic forward modelling. *Geological Society Special Publications*, *167*, 83–103.

Phillips, T. B., Fazlikhani, H., Gawthorpe, R. L., Fossen, H., Jackson, C. A. L., Bell, R. E., Faleide, J. I., & Rotevatn, A. (2019). The influence of structural inheritance and multiphase extension on rift development, the Northern North Sea. *Tectonics*, *38*, 4099–4126. https://doi.org/10.1029/2019tc005756

Ravnås, R., Nøttvedt, A., Steel, R., & Windelstad, J. (2000). Syn-rift sedimentary architectures in the northern North Sea. *Geological Society Special Publications*, *167*, 133–177. https://doi.org/10.1144/GSL.SP.2000.167.01.07

Roberts, A. M., & Holdsworth, R. E. (1999). Linking onshore and offshore structures: Mesozoic extension in the Scottish Highlands. *Journal of the Geological Society*, *156*, 1061–1064. https://doi.org/10.1144/gsjgs.156.6.1061

Roberts, A. M., Yielding, G., Kusznir, N. J., Walker, I. M., & Dorn-Lopez, D. (1995). Quantitative analysis of Triassic extension in the northern Viking Graben. *Journal of the Geological Society*, *152*, 15–26. https://doi.org/10.1144/gsjgs.152.1.0015

Scheiber, T., & Viola, G. (2018). Complex bedrock fracture patterns: A multipronged approach to resolve their evolution in space and time. *Tectonics*, *37*, 1030–1062. https://doi.org/10.1002/2017TC004763

Scheiber, T., Viola, G., van der Lelij, R., Margreth, A., & Schönenberger, J. (2019). Microstructurally-constrained versus bulk fault gouge K-Ar dating. *Journal of Structural Geology*, *127*, 103868. https://doi.org/10.1016/j.jsg.2019.103868

Sibson, R. H. (1977). Fault rocks and fault mechanisms. *Journal of the Geological Society*, *133*, 191–213. https://doi.org/10.1144/gsjgs.133.3.0191

Solum, J. G., van der Pluijm, B. A., & Peacor, D. R. (2005). Neocrystallization, farbrics and age of clay minerals from an exposure of the Moab fault, Utah. *Journal of Structural Geology*, *27*, 1563–1576. https://doi.org/10.1016/j.jsg.2005.05.002

Steel, R., & Ryseth, A. (1990). The Triassic-Early Jurassic succession in the northern North Sea: Megasequence stratigraphy and intra-Triassic tectonics. *Geological Society Special Publication*, *55*, 139–168. https://doi.org/10.1144/GSL.SP.1990.055.01.07

Tartaglia, G., Viola, G., van der Lelij, R., & Scheiber, T. (2020). "Brittle structural facies" analysis: A diagnostic method to unravel and date multiple slip events of long-lived faults. *Earth and Planetary Science*, *545*, 116420. https://doi.org/10.1016/j.epsl.2020.116420

Templeton, J. A. (2015) *Structural evolution of the Hornelen basin (Devonian, Norway) from detrital thermochronology* (p. 243). Colombia University.

Torgersen, E., Viola, G., Zwingmann, H., & Harris, C. (2014). Structural and temporal evolution of a reactivated brittle–ductile fault – Part II: Timing of fault initiation and reactivation by K-Ar dating of

synkinematic illite/muscovite. *Earth and Planetary Science Letters*, *407*, 221–233. https://doi.org/10.1016/j.epsl.2014.09.031

Torgersen, E., Viola, G., Zwingmann, H., & Henderson, I. H. C. (2015). Inclined K-Ar illite age spectra in brittle fault gouges: effects of fault reactivation and wall-rock contamination. *Terra Nova*, *27*(2), 106–113. https://doi.org/10.1111/ter.12136

Torsvik, T. H., Andersen, T. B., Eide, E. A., & Walderhaug, H. J. (1997). The age and tectonic significance of dolerite dykes in western Norway. *Journal of the Geological Society*, *154*, 961–973. https://doi.org/10.1144/gsjgs.154.6.0961

Torsvik, T. H., Sturt, B. A., Swensson, E., Andersen, T. B., & Dewey, J. F. (1992). Palaeomagnetic dating of fault rocks: evidence for Permian and Mesozoic movements and brittle deformation along the extensional Dalsfjord Fault, western Norway. *Geophysical Journal International*, *109*(3), 565–580. https://doi.org/10.1111/j.1365-246X.1992.tb00118.x

Uysal, I. T., Mutlu, H., Altunel, E., Karabacak, V., & Golding, S. D. (2006). Clay mineralogical and isotopic (K–Ar, δ18O, δD) constraints on the evolution of the North Anatolian Fault Zone, Turkey. *Earth and Planetary Science Letters*, *243*, 181–194. https://doi.org/10.1016/j.epsl.2005.12.025

Van der Pluijm, B. A., Hall, C. M., Vrolijk, P. J., Pevear, D. R., & Covey, M. C. (2001). The dating of shallow faults in the earth's crust. *Nature*, *412*, 172–175. https://doi.org/10.1038/35084053

Vermeesch, P. (2018). IsoplotR: A free and open toolbox for geochronology. *Geoscience Frontiers*, *9*, 1479–1493. https://doi.org/10.1016/j.gsf.2018.04.001

Viola, G., Scheiber, T., Fredin, O., Zwingmann, H., Margreth, A., & Knies, J. (2016). Deconvoluting complex structural histories archived in brittle fault zones. *Nature Communications*, *7*, 13448. https://doi.org/10.1038/ncomms13448

Vrolijk, P., Pevear, D., Covey, M., & LaRiviere, A. (2018). Fault gouge dating: History and evolution. *Clay Minerals*, *53*, 305–324. https://doi.org/10.1180/clm.2018.22

Walsh, E. O., Hacker, B. R., Gans, P. B., Grove, M., & Gehrels, G. (2007). Protolith ages and exhumation histories of (ultra)high-pressure rocks across the Western Gneiss Region, Norway. *Geological Society of America Bulletin*, *119*, 289–301.

Walsh, E. O., Hacker, B. R., Gans, P. B., Wong, M. S., & Andersen, T. B. (2013). Crustal exhumation of the Western Gneiss Region UHP terrane, Norway: 40Ar/39Ar thermochronology and fault-slip analysis. *Tectonophysics*, *608*, 1159–1179. https://doi.org/10.1029/2020TC006178

Wiest, J., Wrona, T., Bauck, M. S., Fossen, H., Gawthorpe, R., Osmundsen, P. T., & Faleide, J. I. (2020). From Caledonian collapse to North Sea rift – The extended history of a metamorphic core complex. *Tectonics*, *39*, C006178. https://doi.org/10.1029/2020TC006178

Wilson, R. W., Holdsworth, R. E., Wild, L. E., McCaffrey, K. J. W., England, R. W., Imber, J., & Strachan, R. A. (2010). Basement-influenced rifting and basin development: A reappraisal of post-Caledonian faulting patterns from the North Coast Transfer Zone, Scotland. *Geological Society, London, Special Publications*, *335*, 795–826. https://doi.org/10.1144/SP335.32

Young, D. J., Hacker, B. R., Andersen, T. B., & Gans, P. B. (2011). Structure and 40Ar/39Ar thermochronology of an ultrahigh-pressure transition in western Norway. *Journal of the Geological Society*, *168*, 887–898. https://doi.org/10.1144/0016-76492010-075

Zwingmann, H., & Mancktelow, N. (2004). Timing of alpine fault gouges. *Earth and Planetary Science Letters*, *223*, 415–425. https://doi.org/10.1016/j.epsl.2004.04.041

Zwingmann, H., Mancktelow, N., Antognini, M., & Lucchini, R. (2010). Dating of shallow faults: New constraints from the AlpTransit tunnel site (Switzerland). *Geology*, *38*, 487–490. https://doi.org/10.1130/G30785.1

Zwingmann, H., Yamada, K., & Tagami, T. (2010). Timing of brittle deformation within the Nojima fault zone, Japan. *Chemical Geology*, *275*, 176–185. https://doi.org/10.1016/j.chemgeo.2010.05.006

SUPPORTING INFORMATION

Additional Supporting Information may be found online in the Supporting Information section.